Quantitative evaluation of mineral grains using automated SEM–EDS analysis and its application potential in optically stimulated luminescence dating

Michael C. Meyer [a,b,*], Peter Austin [c], Peter Tropper [d]

[a] Institute for Geology und Palaeontology, University of Innsbruck, Innrain 52f, 6020 Innsbruck, Austria
[b] Centre for Archaeological Science, School of Earth and Environmental Sciences, University of Wollongong, Wollongong, NSW 2522, Australia
[c] CSIRO Process Science & Engineering, Australian Minerals Research Centre, Waterford, WA 6155, Australia
[d] Institute of Mineralogy and Petrography, University of Innsbruck, Innrain 52f, 6020 Innsbruck, Austria

HIGHLIGHTS

- Automated mineralogy system (QEMSCAN) applied to coarse & fine-grained OSL samples.
- Feldspar and mica inclusions frequently observed in purified coarse quartz samples.
- Complex mineralogical composition in fine-grained samples revealed.
- Efficiency of physico-chemical preparation strategies also evaluated via QEMSCAN.
- QEMSCAN useful for quality assurance & investigation of problematic OSL samples.

ARTICLE INFO

ABSTRACT

Optically stimulated luminescence (OSL) dating allows constraining the depositional age of sediments with good accuracy and precision. A fundamental requirement in OSL dating is to use purified sub-samples (i.e. mono-mineralogic aliquots composed of e.g. quartz or potassium feldspar only), because of the different OSL properties and dosimetry characteristics of each mineral phase. Where multiple mineral phases are present on an aliquot, a mixed OSL signal might be obtained, with potentially adverse effects on the robustness of the resulting optical ages. Detailed evaluation of the mineralogical composition of the hundreds or even thousands of individual mineral particles that constitute an aliquot in OSL dating has − until recently − not been reasonably feasible with current analytical techniques.

Here we report on the use of an automated mineralogy system that combines scanning electron microscopy (SEM) and energy dispersive spectroscopy (EDS) and facilitates ultra-fast analysis of particulate mineral phases with a spatial resolution on the micron scale. The method is applied to mono-mineralogic coarse-grained (100–250 μm) and poly-mineral fine-grained (4–11 μm) OSL samples, respectively and cross-checked with electron probe micro analysis (EPMA). It is shown that (i) some coarse-grained mineral extracts that underwent standard physico-chemical preparation to isolate quartz for OSL dating, still suffer from mineralogical contamination, mainly in the form of feldspar and mica inclusions and, that (ii) polymineral fine-grained samples reveal a complex mineralogical composition with a significant percentage of mica (mainly muscovite). Implications of these quantitative mineralogical observations for OSL dating are discussed. QEMSCAN is further used to examine the efficiency of different physico-chemical preparation strategies to isolate a restricted range of mineralogies and to optimize single preparation steps. We conclude that the clear advantage of automated SEM–EDS systems lies in the rapidity with which accurate high-resolution maps of hundreds or even thousands of mineral particles can be generated, i.e. at a level statistically representative of the bulk OSL sample. Automated SEM–EDS techniques might thus be helpful in OSL dating for quality assurance and investigation of problematic OSL samples.

* Corresponding author. Institute for Geology und Palaeontology, University of Innsbruck, Innrain 52f, 6020 Innsbruck, Austria. Tel.: +43 (0) 512 507 5683.
E-mail address: michael.meyer@uibk.ac.at (M.C. Meyer).

1. Introduction

Sedimentary quartz and feldspar grains are natural dosimeters routinely used in the environmental and archaeological sciences for optical dating of sediments. Standard physico-chemical preparation steps (i.e. a combination of acid treatments, sieving and density preparation) are generally applied to extract sediment sub-samples with a restricted range of mineralogies and grain sizes for luminescence analysis. The accuracy and precision of the resulting optically stimulated luminescence (OSL) ages is influenced by the mineralogical composition of these purified sub-samples (aliquots), because different minerals have different dosimetry and luminescence characteristics. Hence, only mono-mineralogical aliquots and grains that lack contaminating mineral inclusions are suitable for optical dating.

Several methods can be used to examine the efficiency and reliability of the physico-chemical preparation steps and the purity of the final mineral extracts. A common routine check is the inspection of aliquots under reflected-light microscopy. However, some mineral phases or microscopic mineral inclusions cannot be identified via that technique and visual checks using reflected-light microscopy are thus of limited use.

Methods that are based solely on the luminescence behaviour of the aliquots to identify some mineral phases have been developed as well. For OSL dating of quartz, tests that involve infrared stimulated luminescence (IRSL) to detect feldspar grains and feldspar inclusions in quartz grains are now part of the dating routine (e.g. Smith et al., 1990; Stokes, 1992; Duller, 2003; Roberts and Wintle, 2003). For single-grain dating of feldspar, pulse annealing methods might be applied to differentiate between potassium (K) and sodium-rich (Na) feldspar grains (Li et al., 2011). Such luminescence-based quality tests are important but already require OSL measurements (some of which are time consuming) and will identify specific but not all contaminating mineral phases that might be present in the bulk sample.

The geochemical and mineralogical composition of a mineral extract can also be studied via X-ray techniques such as X-ray diffraction (XRD) or X-ray fluorescence (XRF) analysis. These methods, however, are (i) destructive (i.e. involve grinding of a few grams of sample material); (ii) XRD is insensitive to amorphous minerals or mineral inclusions and has a detection limit of 1% for crystalline phases which is inadequate for luminescence dating and (iii) via XRF only the chemical (rather than the mineralogical) composition of the bulk sample can be determined (albeit at high precision). Hence, these X-ray techniques are only partly useful for a qualitative and quantitative mineralogical evaluation of an OSL sample.

Chemical data with a high to very high spatial (micron scale) as well as chemical resolution (ppm level) can be obtained via electron probe micro analysis (EPMA), X-ray spectroscopy (e.g. EDS – energy dispersive spectroscopy), or mass spectrometry (e.g. laser ablation inductively couple plasma mass spectrometry – LA ICP-MS). These techniques also allow elemental concentration maps to be generated if the electron or laser beam is scanned over a well-defined sample detail. However, these high-resolution methods can become extremely time-consuming and cost-intensive or even impractical if very large data sets composed of hundreds of thousands of measurement points have to be generated in order to be statistically representative of a bulk sample. Again, these techniques provide chemical rather than mineralogical information.

Over the last two decades automated mineralogy systems have been developed that use scanning electron microscopes (SEM) fitted with multiple X-ray EDS detectors. The concomitant development of automated processing and data presentation software allows ultra-fast analysis of e.g. mineral phase and other inorganic materials and quantification of mineralogical, textural and chemical information on a particle-by-particle basis, with a resolution down to the micron scale. Such automated SEM-EDS systems are now routinely used in the mining industry (e.g. Goodall et al., 2005; Jaime et al., 2009; Benedictus et al., 2008) and have gained popularity in the geo- and environmental (e.g. Pirrie et al., 2003; Martin et al., 2008; Haberlah et al., 2010) as well as in the archaeological sciences (e.g. Knappett et al., 2005; Hardy and Rollinson, 2009). Here we report on the application potential of such an automated SEM-EDS mineralogy approach (i.e. QEMSCAN©) for luminescence dating.

2. Quantitative evaluation of minerals by scanning electron microscopy (QEMSCAN©)

The first automated mineralogy system based on an integrated SEM–EDS technology was developed by CSIRO in Australia and originally termed QEM*SEM© (Sutherland et al., 1988; Sutherland and Gottlieb, 1991). This system has been advanced into a general purpose instrument known under the acronym QEMSCAN© for characterizing ores and to investigate the performance of industrial mining plants. Both, QEMSCAN© and a similar approach named mineral liberation analysis (MLA, developed by the U. Queensland, Australia; Gu and Napier-Munn, 1997; Fandrich et al., 2007) are now available as commercial products offered by FEI Company. Also other groups have developed computer controlled SEM's principally for image analysis applications (e.g. Nuspl et al., 2004; Xie et al., 2005).

The QEMSCAN system typically consists of a SEM equipped with up to four energy dispersive X-ray (EDX) detectors. A large
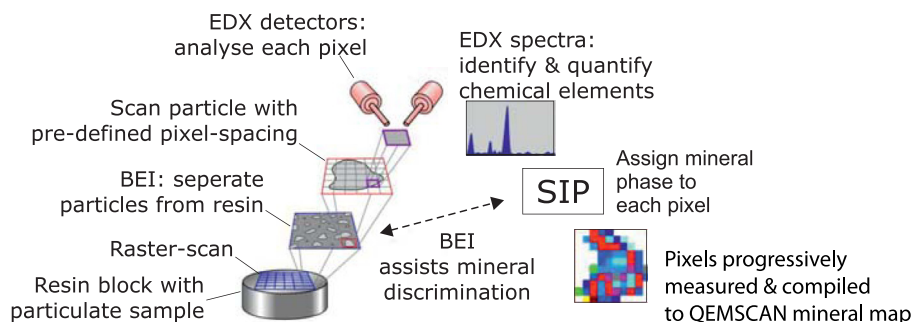
Fig. 1. Schematic workflow of a QEMSCAN analysis using particle mineralogical analysis mode. A backscattered electron image (BEI) is generated from a polished sample block to isolate individual mineral particles via an image analysis routine. Multiple energy-dispersive X-ray (EDX) detectors scan each mineral particle with a pre-defined resolution (pixel spacing). The resulting EDX spectra are automatically analysed and each pixel is assigned to a specific mineral phase via a species identification profile (SIP) allowing accurate mineralogical maps to be generated for each mineral particle.

measurement chamber can accommodate up to 16 sample blocks (i.e. polished rock samples, thin sections or particulate material that has been impregnated with resin, sectioned and polished). Stage control as well as image acquisition are fully automated, thus no operator assistance is required during measuring. The electron beam of the SEM performs a raster or linear scan of the sample surface, generating (amongst other secondary emissions) back-scattered electrons as well as X-ray emissions. From each measurement point the X-ray spectrum is collected via the EDX detectors, while a backscattered electron image (BEI) of the sample surface is compiled via the SEM (Fig. 1). Characteristic peaks in the

X-ray spectrum indicate the presence of a chemical element. Each EDX spectrum is analyzed by windowing, background subtraction, overlap correction, thresholding, and the calculation of peak ratios to resolve individual element spectral lines, thus allowing the chemical composition of each measurement point to be determined. The X-ray data obtained for each point analysis are compared with a database of mineral species (i.e. species identification profile SIP, Fig. 1). This database lists elements that must be present, and elements that may be present in order to assign a pixel to a specific mineral phase. Mineral phases that reveal similar X-ray spectra can be discriminated on the basis of their BEI and/or by
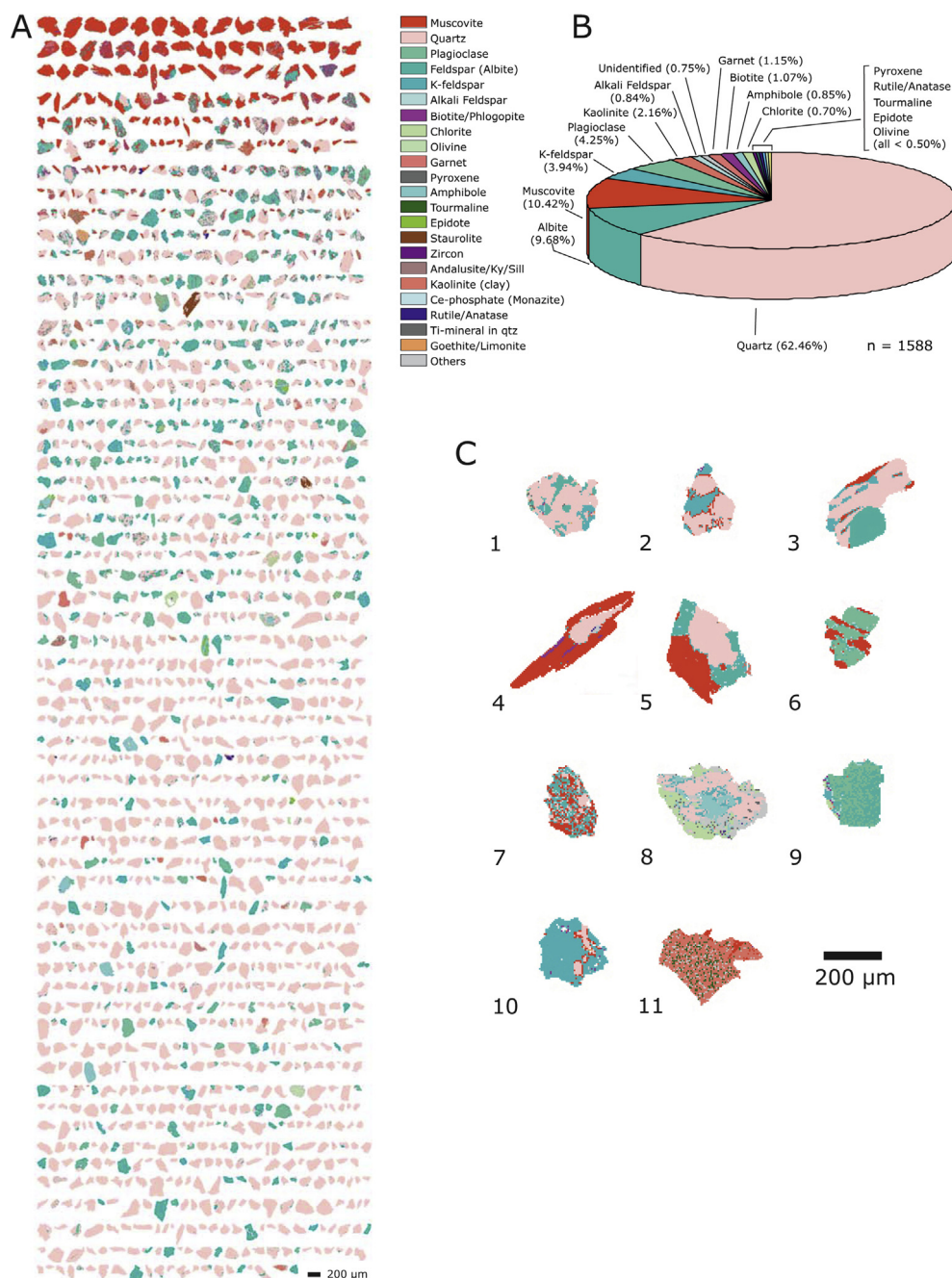
Fig. 2. QEMSCAN results for sample Ph 2305. A: Mineral list ordered by % area of muscovite (*n* = 1588). B: Pie chart of modal sample mineralogy in % area. C: Mineral maps for selected sediment grains. Grain 1 and 2: Quartz grain with feldspar inclusions (i.e. Kfs & albite); Grain 3–5: composite grains composed of quartz, muscovite and feldspar; Grain 6: quartz in association with amphibole, chlorite and Kfs; Grain 7: quartz in association with biotite and feldspar (Kfs & albite). Grains 8–9: sediment grains composed of a fine mosaic of quartz, feldspar and/or muscovite (intermingled mineralogy). Grain 10: feldspar grain with quartz and muscovite inclusions; Grain 11: kaolinite particle.

element ratios. Real-time processing of these EDX and BEI signals thus generates digital images that classify pixels (i.e. measurement points) as mineral phases.

Despite being an automated SEM-EDS technique, QEMSCAN has the same fundamental detection limits as conventional EDS. EDS can determine the elemental concentration for an individual pixel down to around 0.5% (i.e. 5000 ppm), depending on the element and potential overlaps of elemental X-ray spectra. Integration times of a few seconds per pixel are required to achieve these detection limits. A typical QEMSCAN spectrum acquisition has 1000 counts

(as used for the analyses reported here), so the detection limit or chemical resolution is reduced to a few % (i.e. 3–5% depending on the element). Accurate mineralogical maps with a chemical resolution at the % level can be produced, for the sample as a whole, however, because potentially many millions of pixels are analysed.

The nature of the sample and the specific mineralogical problem will determine the spatial scanning resolution (i.e. pixel spacing), the EDS integration time per pixel as well as the mode of QEMSCAN analysis (i.e. amongst others the bulk and the particle mineralogical analysis mode). The bulk mineralogical analysis mode is based on
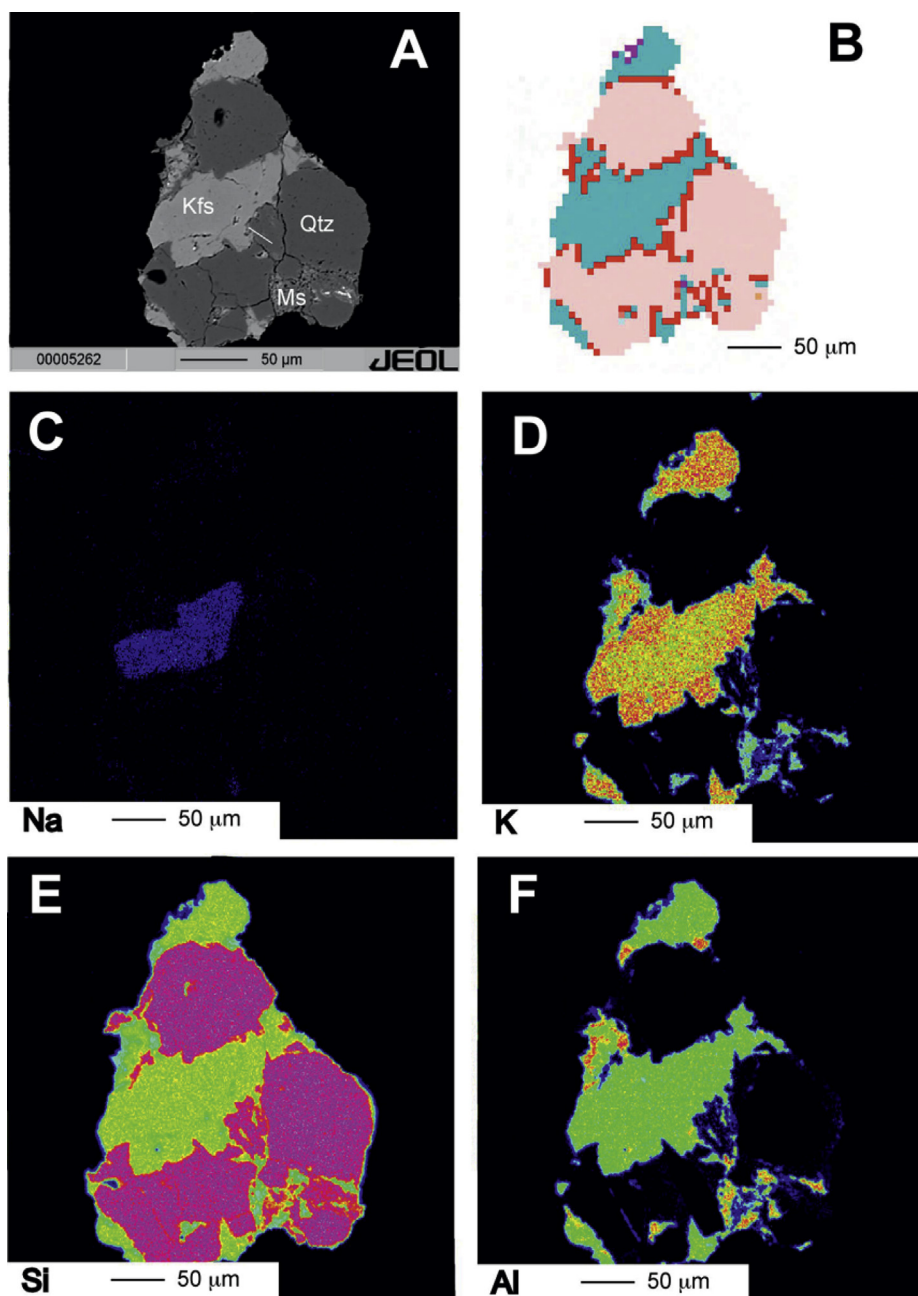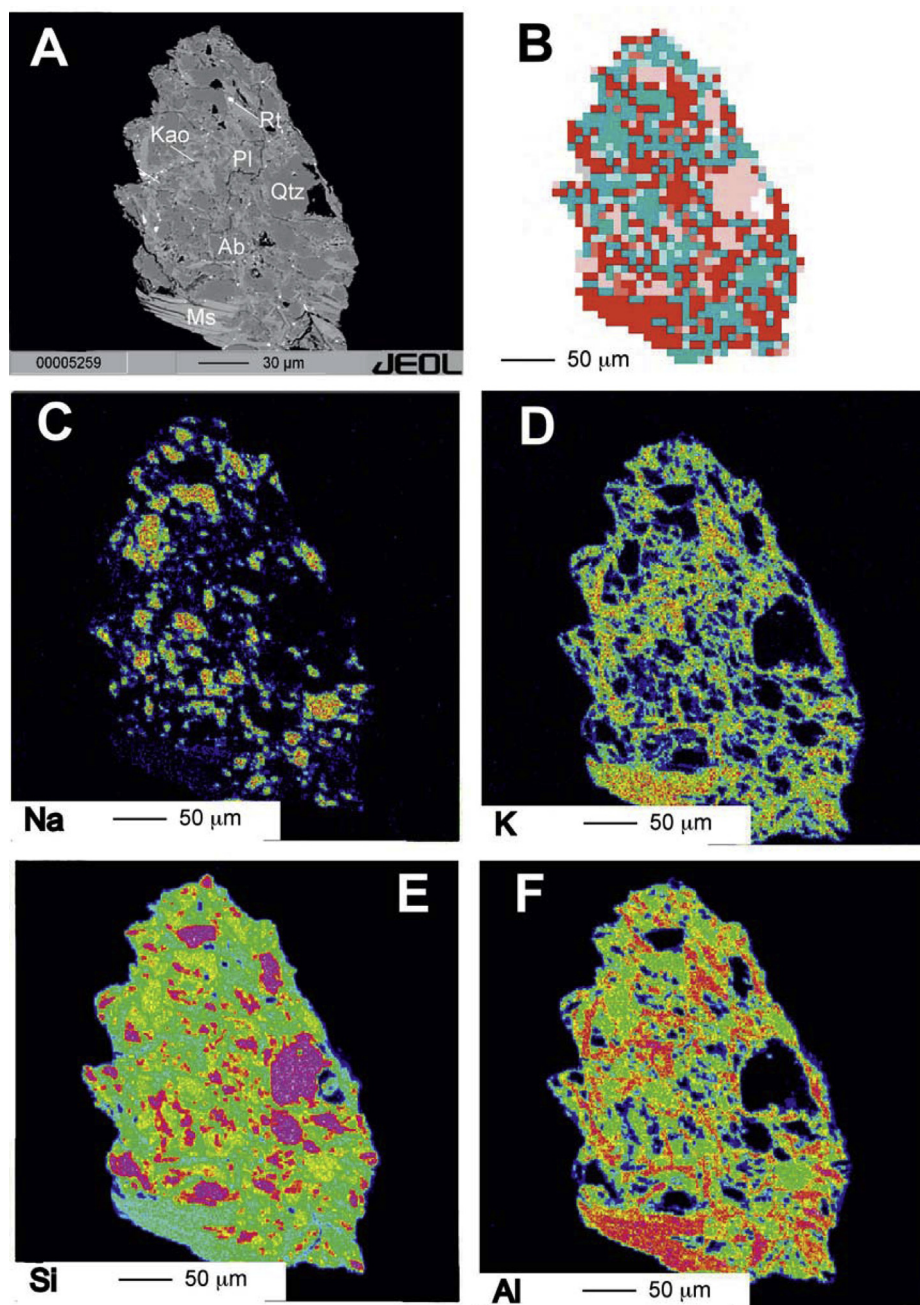

Fig. 3. QEMSCAN – EPMA comparison for grain 2 of sample Ph 2305. A: Backscattered electron (BSE) image of the composite grain; Kfs: K-feldspar; Qtz: quartz; Ms: muscovite. B: QEMSCAN image (grain 2 in Fig. 2C). C–F: X-ray distribution images showing the spatial distribution of characteristic X-rays of selected elements (C: Na distribution; D: K distribution; E: Si distribution; F: Al distribution). C: Na-rich (albite-rich, blue) core in K-feldspar. D: Conversely a low K-content (green–yellow) in the core and a high K content in the rim (red) can be seen in the K-feldspar. The turquoise areas in the lower right of the image correlate with muscovite, which contains less K_2O (ca. 9–11 wt.%) compared with K-feldspar (ca. 14–16 wt.%). E: The high Si areas are pink and correlate well with quartz. The green areas contain less Si and correlate with K-feldspar. F: The small red areas indicate high Al contents (>30 wt.% Al_2O_3) and correlate with muscovite while the green areas indicate low Al contents (<20 wt.% Al_2O_3) and correlate with K-feldspar. (For interpretation of the references to colour in this figure legend, the reader is referred to the web version of this article.)

linear scans and can be used on drill cores, rock and particulate samples, while the particle mineralogical analysis mode is used for detailed mineralogical characterization of particles up to 1 mm. In this mode individual particles are identified on the BEI and scanned via EDX to determine their mineralogy. Here we apply QEMSCAN (using the particle mineralogical analysis mode) to coarse and fine-grained OSL samples, i.e. to particulate samples that range in grain size between 100–250 μm and 4–11 μm, respectively. In addition, electron microprobe analysis (EMPA) is used to cross-check the

QEMSCAN results for selected grains in the coarse grain-size fraction.

3. OSL sample preparation, QEMSCAN and EMPA analysis – methodological aspects

All samples in this study are unlithified Quaternary sediments, either from a proglacial environment (i.e. the coarse-grained samples PH 2305 and CHM 1) or a lacustrine sedimentary context

Fig. 4. QEMSCAN – EPMA comparison for grain 7 of sample Ph 2305. A: Backscattered electron (BSE) image of the composite grain; Pl: plagioclase; Qtz: quartz; Ms: muscovite; Rt: rutile; Kao: kaolinite. B: QEMSCAN image (grain 7 in Fig. 2C). C–F: X-ray distribution images showing the spatial distribution of characteristic X-rays of selected elements (C: Na distribution; D: K distribution; E: Si distribution; F: Al distribution). C: The Na-rich areas (red, >10 wt.% Na$_2$O) correlate with albite and the low Na areas (blue, ca. 1–2 wt.% Na$_2$O) correlate with muscovite. D: Conversely high K-contents (red–yellow, ca. 9–11 wt.% K$_2$O) correlate with muscovite. E: The high Si areas are pink and correlate well with quartz. The green–yellow areas contain less Si and correlate with albite and the turquoise areas (e.g. lower left) correlate with muscovite. F: The red areas indicate high Al contents (>30 wt.% Al$_2$O$_3$) and correlate with muscovite while the green areas indicate low Al contents (<20 wt.% Al$_2$O$_3$) and correlate with K-feldspar. The black areas within the composite grain correlate with quartz. (For interpretation of the references to colour in this figure legend, the reader is referred to the web version of this article.)
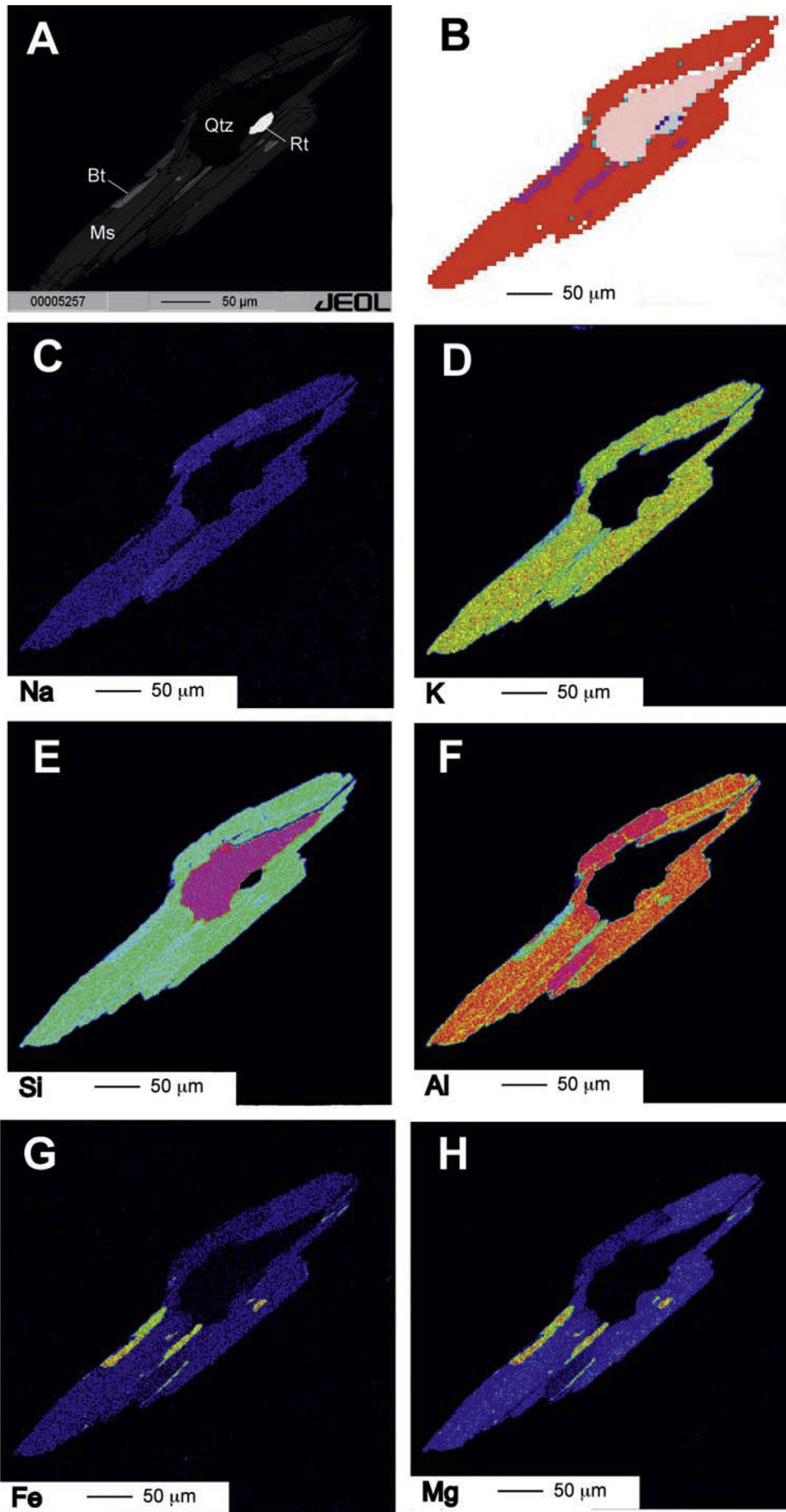
(i.e. the fine-grained samples NW 11 and THG 04). Sample Ph 2305 is from the Pohorje region (northern Slovenia), NW 11 was taken from Niederwenningen (northern Switzerland, near Zürich), while sample THG 04 was retrieved from the Thalgut gravel pit (northern Switzerland, near Bern). Sample CHM 1 is from the Altai Mountains (Chagan section, Siberia). In all catchments metamorphic and igneous rocks are dominating the geology. We used standard physico-chemical preparation techniques to purify either coarse-grained quartz or polymineral fine grains. All samples were etched with hydrochloric acid and hydrogen peroxide to dissolve any carbonates and organic material. For the coarse-grained samples (i.e. Ph 2305 and CHM 1), sieving and density preparation were used to isolate quartz of the desired size-range from the bulk sample (i.e. sodium polytungstate with a density of 2.62 g/cm³ was used to separate feldspar from quartz and the heavy minerals; a density of 2.75 g/cm³ was used to isolate quartz from the heavy minerals). Subsequently, the quartz extracts were etched for 40 min in 30% hydrofluoric (HF) acid to remove the outer ∼20 μm thick rim of the quartz grains and any remaining feldspar contaminations. Etching with 10% hydrochloric acid was applied to dissolve any fluorides that might have formed during the HF etch. Polymineral fine grain extracts were prepared for the samples NW 11 and THG 4 via settling in Atterberg cylinders using Stokes' law.

For QEMSCAN© analysis (performed at CSIRO Australian Minerals Research Centre, Western Australia) sub-samples between 4 and 0.2 g were prepared. Small sub-samples contained a few hundred particles only and were thus prepared as thin sections bonded to microscope slides (i.e. the grains were sprinkled on resin, cured and carefully polished). Samples with sufficient particle numbers were blended with similar sized graphite particles to disperse the particles. The graphite dispersed particles were vacuum impregnated with resin, cured, sectioned and polished. Prepared samples were coated with carbon using an evaporative carbon coater to prevent charging during analysis with the QEMSCAN©.

All prepared blocks were analyzed with a QEMSCAN© E430. Particle mineralogical analysis scans were used for all samples. An image analysis routine was applied to segregate the particles that have been identified on the BEI from the resin background. The set of pixels corresponding to each particle were then targeted for analysis via EDX. Because the samples that were prepared as thin sections had not been dispersed by graphite, multiple particle contacts were present in their BEI. Without correction, this would have caused the software to interpret the sample as a single particle rather than a set of smaller particles. Consequently, a QEMSCAN© software process to recognize and separate touching particles prior to analysis was used for these samples. The graphite dispersion made this process unnecessary for the samples prepared in resin blocks.

Pixel spacing varied with particle size. Samples with mean sizes over 100 μm were analysed with 4.88 μm pixel spacing, while finer samples were analysed at 0.98 μm pixel spacing. Data acquisition was terminated either when the entire block or thin section was scanned, or in excess of 5000 particles had been analysed. As usual with QEMSCAN© analysis, results are presented in mineral lists and via mineral maps for all scanned particles (Fig. 2). In this study, we further generated a report of the bulk mineralogy, the total number of particles, the number of particles containing specific mineral inclusions, and various particle mineral images to emphasize different aspects of the sample analysis.

A JEOL 8100 SUPERPROBE electron microprobe was used for analysing the mineral compositions by using backscattered electron images (BSE) and X-ray distribution images at the Institute of Mineralogy and Petrography at the University of Innsbruck. Analytical conditions were 15 kV acceleration voltage and 10 nA beam current. This machine is equipped with five wave-length dispersive spectrometers (WDS) thus recording the X-ray intensities of five elements simultaneously. The grains were analysed using squares with sizes from 220 × 220 pixels (grain 4) up to 420 × 420 pixels (grain 1). Pixel size ranged from 0.75 to 1 μm and counting time was 40 msec.

4. QEMSCAN and EPMA results

4.1. Coarse grain quartz samples

Fig. 2 illustrates the QEMSCAN data from a particulate sediment sample (Ph2305, 1588 scanned grains) that has been treated with 10% hydrochloric acid and 10% peroxide, respectively and sieved to a grain size of 180–212 μm (no density preparation or HF etching). The maps of the individual mineral particles are sorted according to mineral grains that report to the mica phase (i.e. muscovite, area %). In this sample and at this stage of sample preparation quartz is the dominant mineral phase (62.5%), but a significant amount of feldspar (i.e. albite, K-feldspar, plagioclase, alkali-feldspar; 18.7% in total), muscovite (10.4%), clay particles (i.e. kaolinite, 2.2%) as well as a range of heavy minerals (∼5.5% in total) is present too (Fig. 2B). A closer examination of the individual QEMSCAN particle images reveals that ∼50% or more of the mineral grains are either composite grains or reveal some sort of mineral inclusions (Fig. 2C). Quartz phases can be found frequently in association with feldspar (e.g. Fig. 2C, grain 1 and 2) or as composite grains with quartz, muscovite and/or feldspar as constituting mineralogical phases (e.g. Fig. 2C, grain 3–5). Composite grains that contain quartz in combination with other mineralogical phases than muscovite or feldspar also exist but are less common (Fig. 2C, e.g. grain 8). Finally, sediment grains composed of multiple mineral phases but with a fine mosaic-like appearance (quartz, feldspar and mica intermingled) can also be found in the QEMSCAN mineral maps (Fig. 2C, e.g. grain 7 and 10).

From this sample 6 mineral grains were selected (i.e. grain 2, 4, 6, 7, 9 and 10 from Fig. 2C) which were also analysed with the electron microprobe at a spatial resolution between 0.75 and 1 μm in order to evaluate the accuracy and precision of the QEMSCAN results independently (Figs. 3–5 and Supplement 1). Fig. 3 shows the comparison between EMPA and QEMSCAN data of a composite grain (i.e. grain 2 from Fig. 2C). The BSE image and the X-ray distribution images of K, Si and Al clearly reveal an intergrowth between K-feldspar and quartz, which is also clearly shown in the QEMSCAN image. Nonetheless an interesting feature is visible in

Fig. 5. QEMSCAN − EPMA comparison for grain 4 of sample Ph 2305. A: Backscattered electron (BSE) image of the composite grain; Bt: biotite; Qtz: quartz; Ms: muscovite; Rt: rutile. B: QEMSCAN image (grain 4 in Fig. 2C). C–H: X-ray distribution images showing the spatial distribution of characteristic X-rays of selected elements (C: Na distribution; D: K distribution; E: Si distribution; F: Al distribution; G: Fe; H: Mg). C: The Na-bearing areas (blue, 1–2 wt.% Na_2O) correlate with muscovite. D: High K-contents (yellow, ca. 9–11 wt.% K_2O) also correlate with muscovite. The black areas within the composite grain correlate with quartz and rutile. E: The high Si areas are pink and correlate with quartz, the green areas correlate with muscovite. The turquoise areas (lamellae at the rim or within the muscovite) contain slightly less Si and correlate with biotite. The black areas within the composite grain correlate with quartz and rutile. F: The red areas indicate high Al contents (>30 wt.% Al_2O_3) show an irregular distribution and correlate with muscovite while the green–turquoise areas indicate lower Al contents (<30 wt.% Al_2O_3) and correlate with biotite. The black areas within the composite grain correlate with quartz and rutile. G, F: The blue areas (low Fe, Mg) correlate with muscovite and the green–yellow areas correlate with high Fe, Mg areas and correlate with biotite lamellae. The black areas within the composite grain correlate with quartz and rutile. (For interpretation of the references to colour in this figure legend, the reader is referred to the web version of this article.)
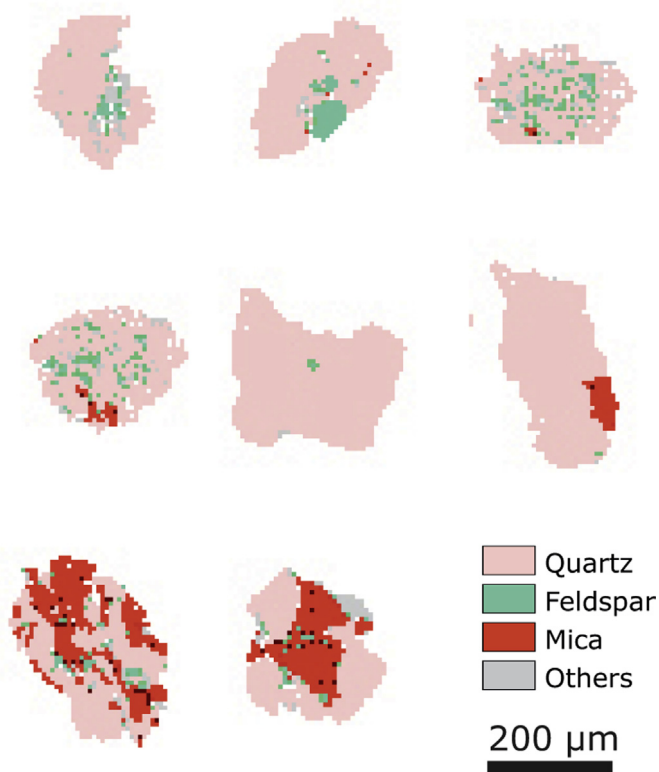
Fig. 6. QEMSCAN mineral maps for selected sediment grains from sample CHM 1.

inconsistencies occur only in the distribution of the K- and Na-bearing feldspars, which is mostly due to an overlap of EDS spectra. In contrast, Fig. 5, an intergrowth between muscovite, quartz, rutile and biotite (i.e. grain 4 from Fig. 2C), shows excellent agreement between the electron microprobe data and the QEMSCAN data and a very high degree of consistency between both methods exists for the other scanned mineral grains as well (Supplement 1).

Sample CHM 1 is a quartz extract that revealed a notoriously problematic OSL behaviour (i.e. a strong IRSL response suggestive of some sort feldspar contamination that rendered OSL dating impossible). An average infrared (IR)-OSL depletion ratio of 0.61 ± 0.21 ($n = 6$) has been obtained despite density preparation ($2.62 < \rho < 2.70$ g/cm^3) and HF etching (40% HF for 40 and 80 min, respectively) and repeating these steps (i.e. an additional 40 min etch with 40% HF and density preparation) did not result in any improvements (IR-OSL depletion ratio of 0.63 ± 0.16 ($n = 16$)). QEMSCAN mineral maps for 1038 particles were obtained for this sample and a modal mineralogy distribution was generated. Quartz dominates the sample (94.4%), followed by muscovite (2.4%), feldspar (1.1%) while traces of other minerals amount to 2.1%. Both, the feldspar and mica phases are encountered as inclusions in quartz particles or form composite grains (Fig. 6). We conducted an additional experiment on CHM 1. A sub-sample was crushed and milled to <11 μm and treated with 37% hexafluorsilicic acid for seven days (to crack-open and dissolve potential feldspar inclusions) and the resulting IR-OSL depletion ratio increased to 0.97 ± 0.3 ($n = 2$). This experiment supports the QEMSCAN observation that feldspar (but also mica) phases can survive OSL sample preparation and standard acid treatments in the form of inclusions in quartz grains that in turn might be responsible for aberrant OSL behaviour of some quartz aliquots.

Although not discussed here in detail, further QEMSCAN analyses on additional coarse-grained samples suggest that feldspar and mica inclusions in quartz grains as well as composite grains can persist in the dating fraction of some samples. The concentration of these contaminating mineral phases usually decreases with more rigorous separation techniques (e.g. via double density preparation and additional etching with HF or hexafluorsilicic acids usually to <1% in most cases). However, the impact of such mineralogical contaminations on the accuracy and precision of OSL ages has yet to be investigated for each of those samples in more detail.

4.2. Polymineral fine-grained samples

Two fine-grained (i.e. 4–11 μm) OSL samples were scanned and the results are shown in Fig. 7 (dating fraction of THG 4 and NW 11,

the QEMSCAN image, namely a small zone of muscovite occurs between K-feldspar and quartz in the central part of the image (Fig. 3B). This feature cannot be explained by the X-ray distribution images since the Si and Al content shows no spatial variations (Fig. 3E and F), thus it has to be assumed that this small zone results from a mixture of the EDS spectra of muscovite and quartz, which could indeed produce a muscovite-like EDS spectrum. On the other hand, QEMSCAN reproduces nicely the muscovites in the lower right part of the composite grain (compare e.g. Fig. 3B and F). Fig. 4 shows the comparison between both methods in a complex aggregate (i.e. grain 7 from Fig. 2C), which represents an intergrowth between K-feldspar, albite, muscovite and quartz. When comparing the BSE image and the QUEMSCAN image it is obvious that a large degree of agreement exists. The X-ray distribution of K, Al and Si images also reveal that the spatial distribution of quartz and muscovite is largely correct in the QEMSCAN image. Small
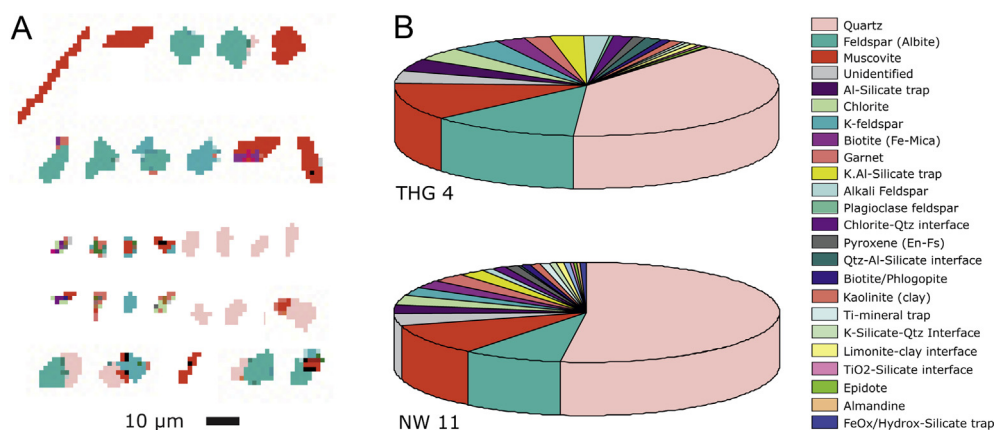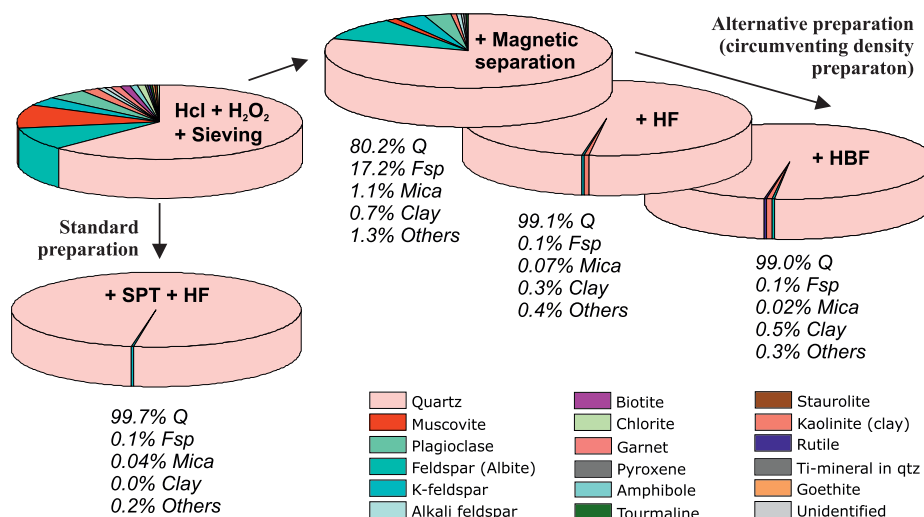

Fig. 7. A: QEMSCAN mineral maps for selected sediment grains from fine-grained sample THG 4. B: Modal mineralogies (% area) of the fine-grained samples THG 4 and NW 11.

Fig. 8. Modal mineralogies after specific physico-chemical preparation steps (QEMSCANs of sample Ph 2305). The first pie chart (top left) was made after the sample has been treated with HCl, H_2O_2 and sieved to a grain size of 180−212 μm. Vertical path: standard preparation − density preparation (sodium polytungstate; $2.62 < \rho < 2.70$ g/cm^3) and HF acid treatment for 40 min. Horizontal path: alternative preparation − magnetic separation and HF etching for 40 min (further etching with HBF is optional and did not improve the results for sample Ph 2305).

respectively; Lowick et al., 2012). In these samples about 40−50% of the bulk sample is composed of quartz, while the feldspar content varies between 10 and 20% (2−4% K-feldspar) and the mica amounts to ∼10%. A wide range of further silicate minerals are present at the % level in these samples too (i.e. mainly heavy minerals with concentrations between 1 and 4%; Fig. 7 and Supplement 2). Scanning these fine-grained samples with a pixel spacing of 0.98 μm (i.e. the maximum scanning resolution of QEMSCAN) ensured that even the smallest grains are mapped via multiple measurement points (i.e. 4 μm grains are defined by at least 2−4 pixels while the fast majority of particles are represented by ∼10−40 pixels; Fig. 7). However, a high percentage of unidentified pixels are apparent in the modal pie charts of these fine-grained samples too, e.g. 4% in the case of THG 4 and NW 11 (i.e. an order of magnitude higher than for any coarse-grained sample). The reason lies in the small grain size of these samples and the volume of the sample that has been excited by the electron beam during EDX analysis (i.e. ∼2 μm wide and deep). As a result, mixed EDS spectra are easily obtained along e.g. grain boundaries due to the grain-to-grain contacts or grain-resin contacts or because of the presence of additional mineral phases at greater depth. Hence, if there are two or more mineral phases present within that diameter (and depth) of the electron beam location, then a mixed spectrum containing contributions form two or more minerals is generated. In most instances these mixed spectra do not match an entry in the SIP and the corresponding pixels are thus reported as unidentified. This phenomenon is more apparent when the grain size gets closer to the spatial resolution i.e. in finer grained samples.

Despite these limitations, mineral inclusions and composite grains can be observed in the coarser grains of the fine grain dating fraction as well (Fig. 7). Furthermore, the substantial number of scanned grains per sample (i.e. 6932 and 8628 grains for sample THG 4 and NW 11, respectively) ensures that the modal mineralogy distribution is representative of the bulk sample.

4.3. Physico-chemical sample preparation procedure

We also examined the efficiency of different preparation strategies in purifying coarse-grained quartz extracts from the bulk sample using QEMSCAN. Sub-samples of Ph2304 were treated with

HCl, H_2O_2 and sieved to 180−212 μm followed by (i) density preparation using sodium polytungstate (i.e. standard preparation as outlined above; Fig. 8 −vertical path) and alternatively (ii) via magnetic separation (using a Franz Magnetic Separator) and HF etching (no density preparation; Fig. 8 − horizontal path). Standard preparation techniques for this sample resulted in a mineral extract consisting to 99.7% of quartz (0.1% feldspar, 0.04% mica and 0.1% other minerals). A similar purity was achieved via a combination of magnetic separation and fluorsilicic acid treatment (30% HF for 40 min), while an additional treatment with fluoroboric acid (45% HBF_4 for 3 days) did not result in any further improvements (Fig. 8). These results suggest that the labour- and time-consuming procedure of density preparation could be successfully circumvented via magnetic separation and HF etching, at least for sample Ph 2305.

5. Discussion and conclusions

The mineral maps produced in this preliminary QEMSCAN study demonstrate that feldspar and mica can persist in the coarse-grained quartz dating fraction of OSL samples, despite rigorous preparation and purification attempts, mainly in the form of inclusions. Most other mineral phases (heavy minerals, clay minerals) were removed successfully or reduced (in most instances) to negligible concentrations (i.e. <1%). Feldspar and mica phases have been found in coarse-grained quartz extracts in three forms: a) as simple discrete inclusions, b) finely intermingled with quartz or c) in the form of composite grains (i.e. individual particles composed of relatively large sub-grains of quartz, feldspar and/or mica; Figs. 2C and 6). The same grain-types and inclusions have been recognized in the dating fraction of fine-grained OSL samples as well. A detailed comparison of QEMSCAN and electron microprobe data (BSE, X-ray distribution) obtained for selected coarse grains shows a very good agreement between both methods, suggesting that QEMSCAN is capable of providing accurate mineral maps of high spatial resolution in the context of OSL dating.

QEMSCAN data confirm the complex mineralogical composition of polymineralic fine-grained samples. A significant percentage of the pixels in the QEMSCAN mineral lists of the two polymineral fine-grained samples studied here report to the feldspar (∼40−50%) and mica phase (∼10%). Heavy minerals and clay particles are

present at concentrations between ∼4% and 1% (Fig. 7). It can be expected that such mineral mixtures have extremely complex luminescence and paleodosimetric characteristics, rendering OSL dating of polymineral samples challenging.

Various measurement protocols that use IR stimulation to account for feldspar contamination in coarse grain quartz extracts as well as in aliquots composed of polymineral fine grains have been put forward (e.g. Roberts and Wintle, 2003; Duller, 2003). Quartz is routinely stimulated with blue LEDs (centered at a wavelength of 470 nm) while luminescence detection is in the UV band (i.e. between ∼270 and 380 nm). Where a significant IRSL signal is obtained in the quartz detection window (270–380 nm), it is assumed that this originates from feldspars (as quartz does not respond to stimulation with IR).

The luminescence properties of mica have not been explored in full detail yet, but the existing literature suggests that mica (i) can give a natural as well as regenerated luminescence signal under both, blue light and IR stimulation (Clark and Sanderson, 1994; Kortekaas and Murraya, 2005; Li and Yin, 2006), (ii) possesses thermoluminescence (TL) emission bands at various temperatures (e.g. Kristianpoller et al., 1988; Krbetschek et al., 1997; Soliman, 2003; Ige et al., 2006; Lakhwant et al., 2012) and (iii) reveals luminescence properties that can vary from sample to sample (Kortekaas and Murraya, 2005; Clark and Sanderson, 1994). Hence, an IRSL response from a quartz aliquot does not necessarily imply the presence of feldspar but could also be due to some mica contamination (or both). Moreover, single aliquot regenerative (SAR) growth curves have been constructed for sedimentary mica by Kortekaas and Murraya (2005; stimulation in the blue and detection in the UV band) and it has been found that saturation occurs at much higher doses than for quartz (i.e. >800 Gy). OSL ages that derive from samples that contain mica in the dating fraction (and in particular older samples with mica contamination) should thus be treated with caution. The fact that mica contamination is not always readily identifiable in the dating fraction of a sample (neither macroscopically nor via its luminescence properties) adds difficulty to that problem. QEMSCAN might be an analytical tool that can help elucidating the exact mineralogical composition of given quartz extracts, thus narrowing down the potential source for an aberrant OSL behaviour in some samples.

A routine QEMSCAN run detects elements on the % level (chemical resolution of 3–5%), while significantly longer integration times at the EDS detectors are required to push for the ppm level (i.e. by a factor of 10 and more to achieve a chemical resolution of several hundred to several thousand ppm). Hence, determining e.g. the precise potassium content for a larger set of individual feldspar grains (their K concentrations can range from 0 to 14%), as required for single-grain feldspar dating, would theoretically be feasible using QEMSCAN. An exact quantification of the uranium, thorium and potassium concentrations at the ppm to ppb level for each pixel of a mineral map (as would be required for solving microdosimetry issues in the context of single-grain OSL dating, spatially resolved OSL dating and OSL surface dating) is, however, out of reach with current automated SEM–EDS techniques.

In summary we believe that the clear advantage of QEMSCAN lies in the capability to rapidly generate accurate mineral maps for hundreds or even thousands of individual particles (i.e. at a level statistically representative of the bulk sample) at a high to very-high spatial resolution. This allows the mineralogical composition of OSL samples and contamination issues to be quantified and investigated in more detail than has hitherto been possible. QEMSCAN is also a convenient tool to monitor the quality and efficiency of the physico-chemical preparation steps in the OSL sample purification procedure.

Acknowledgements

Appendix A. Supplementary data

Supplementary data related to this article can be found at http://dx.doi.org/10.1016/j.radmeas.2013.07.004.

References

Benedictus, A., Berendsen, P., Hagni, A.M., 2008. Quantitative characterisation of processed phlogopite ore from Silver City Dome District, Kansas, USA, by automated mineralogy. Minerals Engineering 21, 1083–1093.

Clark, R.J., Sanderson, D.C.W., 1994. Photostimulated luminescence excitation spectroscopy of feldspars in micas. Radiation Measurements 23, 641–646.

Duller, G.A.T., 2003. Distinguishing quartz and feldspar in single grain luminescence measurements. Radiation Measurements 37, 161–165.

Fandrich, R., Gu, Y., Burrows, D., Moeller, K., 2007. Modern SEM-based mineral liberation analysis. International Journal of Mineral Processing 84, 310–320.

Goodall, W.R., Scales, P.J., Butcher, A.R., 2005. The use of QEMSCAN and diagnostic leaching in the characterisation of visible gold in complex ores. Minerals Engineering 18, 877–886.

Gu, Y., Napier-Munn, T., 1997. JK/Philips mineral liberation analyser – an introduction. In: Minerals Processing '97 Conf. Cape Town, SA, p. 2.

Haberlah, D., Williams, M.A.J., Halverson, G., McTainsh, G.H., Hill, S.M., Hrstka, T., Jaime, P., Butcher, A.R., Glasby, P., 2010. Loess and floods: high-resolution multi-proxy data of Last Glacial Maximum (LGM) slackwater deposition in the Flinders Ranges, semi-arid South Australia. Quaternary Science Review 29, 2673–2693.

Hardy, A.D., Rollinson, G.K., 2009. Green eye cosmetics of antiquity. Pharmaceutical Historian 36, 2–7.

Ige, O.A., Tubosun, I.A., Ogundare, F.O., Mokobia, C.E., Balogun, F.A., 2006. TL response of muscovite samples from granite gematite of Ilesa and Ijero-Ekiti, Southwest Nigeria. Radiation Measurements 41, 967–970.

Jaime, P., Gottlieb, P., Butcher, A., Dobbe, R., 2009. The applicability of automated mineralogy on process planning, process optimization, quality control, audit studies and trouble shooting, with emphasis on process plants. Proceedings of Process Mineralogy 78, 1–10.

Knappett, C., Pirrie, D., Power, M.R., Nikolakopoulou, I., Hilditch, J., Rollinson, G.K., 2005. Mineralogical analysis and provenancing of ancient ceramics using automated SEM-EDS analysis (QEMSCAN): a pilot study on LB I pottery from Akrotiri, Thera. Journal of Archaeological Sciences 38, 219–232.

Kortekaas, M., Murraya, A., 2005. A method for the removal of mica from quartz separates. Ancient TL 23, 43–46.

Krbetschek, M.R., Götze, J., Dietrich, A., Trautmann, T., 1997. Spectral information from minerals relevant for luminescence dating. Radiation Measurements 27, 695–748.

Kristianpoller, N., Kirsh, Y., Shoval, S., Weiss, D., Chen, R., 1988. Thermoluminescent properties of mica. Nuclear Tracks and Radiation Measurements 14, 101–104.

Lakhwant, S., Navjeet, K., Mohan, S., 2012. Thermoluminescence characteristics of high gamma dose irradiated muscovite mica. Indian Journal of Pure and Applied Physics 50, 14–18.

Li, S.H., Yin, G.M., 2006. Luminescence properties of biotite relevant to dating and dosimetry. Journal of Luminescence 21, 51–56.

Li, B., Li, S.H., Duller, G.A.T., Wintle, A.G., 2011. Infrared stimulated luminescence measurements of single-grains of K-rich feldspar for isochron dating. Quaternary Geochronology 6, 71–81.

Lowick, S.E., Trauerstein, M., Preusser, F., 2012. Testing the application of post IR-IRSL dating to fine grain waterlain sediments. Quaternary Geochronology 8, 33–40.

Martin, R.S., Mather, T.A., Pyle, D.M., Power, M., Allen, A.G., Aiuppa, A., Horwell, C.J., Ward, E.P.W., 2008. Composition-resolved size distribution of volcanic aerosols in the Mt. Etna plumes. Journal of Geophysical Research 113 (D-17211), 17.

Nuspl, M., Wegscheider, W., Angeli, J., Posch, W., Mayr, M., 2004. Qualitative and quantitative determination of micro-inclusions by automated SEM/EDX analysis. Analytical and Bioanalytical Chemistry 379, 640–645.

Pirrie, D., Power, M.R., Rollinson, G., Camm, G.S., Hughes, S.H., 2003. The spatial distribution and source of arsenic, copper, tin and zinc within the surface sediments of the Fal Estuary, Cornwall, UK. Sedimentology 50, 579–595.

Roberts, H.M., Wintle, A.G., 2003. Luminescence sensitivity changes of polymineral fine grains during IRSL and [post–IR] OSL measurements. Radiation Measurements 37, 661–671.

Smith, B.W., Rhodes, E.J., Stokes, S., Spooner, N.A., 1990. The optical dating of sediments using quartz. Radiation Protection Dosimetry 34, 75–78.

Soliman, C., 2003. Some luminescence properties of the blue emission band of muscovite. Radiation Effects and Defects in Solids 158, 667–673.

Stokes, S., 1992. Optical dating of young (modern) sediments using quartz: results from a selection of depositional environments. Quaternary Science Review 11, 153–159.

Sutherland, D., Gottlieb, P., 1991. Application of automated quantitative mineralogy in mineral processing. Mineral Engineering 4, 753–762.

Sutherland, D., Gottlieb, P., Jackson, R., Willkie, G., Steward, P., 1988. Measurement in section of particles of known composition. Mineral Engineering 1, 317–326.

Xie, R.K., Seip, H.M., Leinum, J.R., Winje, T., Xiao, J.S., 2005. Chemical characterisation of individual particles (PM10) from ambient air in Guiyang City, China. Science of the Total Environment 343, 261–272.